Atmos. Chem. Phys. Discuss., 14, 13869–13908, 2014
www.atmos-chem-phys-discuss.net/14/13869/2014/
doi:10.5194/acpd-14-13869-2014

Atmospheric Chemistry and Physics Discussions
Open Access

Natural or anthropogenic? On the origin of atmospheric sulfate deposition in the Andes of southeastern Ecuador

S. Makowski Giannoni, R. Rollenbeck, K. Trachte, and J. Bendix

Laboratory for Climatology and Remote Sensing (LCRS), Faculty of Geography, University of Marburg, Deutschhausstr. 12, 35032 Marburg, Germany

Received: 4 March 2014 – Accepted: 6 May 2014 – Published: 27 May 2014

Correspondence to: S. Makowski Giannoni (sandro.makowski@posteo.org)

Published by Copernicus Publications on behalf of the European Geosciences Union.

Abstract

Atmospheric sulfur deposition above certain limits can represent a threat to tropical forests, causing nutrient imbalances and mobilizing toxic elements that impact biodiversity and forest productivity. Atmospheric sources of sulfur deposited by precipitation have being roughly identified in only a few lowland tropical forests. Even scarcer are these type of studies in tropical mountain forests, many of them megadiversity hotspots and especially vulnerable to acidic deposition. Here, the topographic complexity and related streamflow condition the origin, type, and intensity of deposition. Furthermore, in regions with a variety of natural and anthropogenic sulfur sources, like active volcanoes and biomass-burning, no source-emission data has been used for determining the contribution of each of them to the deposition. The main goal of the current study is to evaluate sulfate (SO_4^-) deposition by rain and occult precipitation at two topographic locations in a tropical mountain forest of southern Ecuador, and to trace back the deposition to possible emission sources applying back trajectory modeling. To link upwind natural (volcanic) and anthropogenic (urban/industrial and biomass-burning) sulfur emissions and observed sulfate deposition, we employed state of the art inventory and satellite data, including volcanic passive degassing as well. We conclude that biomass-burning sources generally dominate sulfate deposition at the evaluated sites. Minor sulfate transport occurs during the shifting of the predominant winds to the north and west. Occult precipitation sulfate deposition and likely rain sulfate deposition are mainly linked to biomass-burning emissions from the Amazon lowlands. Volcanic and anthropogenic emissions from the north and west contribute to occult precipitation sulfate deposition at the mountain crest *Cerro del Consuelo* meteorological station and to rain-deposited sulfate at the upriver mountain-pass *El Tiro* meteorological station.

ACPD
14, 13869–13908, 2014

1 Introduction

Sulfur enters the atmosphere principally as sulfur dioxide (SO_2), an air pollutant with a lifetime of about one to two days, before it is normally deposited or oxidized to sulfate (SO_4^-). After oxidation, lifetime increases to three or more days, depending on the state of the atmosphere and the injection height. Because of its longer life time, sulfate can be spread over greater distances. In high concentrations, sulfate decreases the pH of precipitation to levels that represent a threat to health and ecosystems. This phenomenon called "acid rain" was discussed in the past, particularly in the industrialized countries of Europe and North America where adverse effects were found more serious for health than for ecosystems (Menz and Seip, 2004).

In tropical ecosystems, only few studies are available despite the fact that they are mostly characterized by an interference-prone biogeochemical cycle and nutrient limitation (Elser et al., 2007; Wullaert et al., 2010), and hence particularly sensitive to acid deposition (Boy et al., 2008; Delmelle et al., 2002). Kuylenstierna et al. (2001), for example, revealed that acidification from atmospheric sulfur could represent a threat to tropical ecosystems in developing countries. Acidification of soils due to persistent increase in sulfate inputs could lead to nutrient imbalances and changes in ecosystem diversity and productivity (Greaver et al., 2012; Phoenix et al., 2006). It can also mobilize many potentially toxic elements that promote soil degradation and erosion in some areas. Acid and toxic elements can leach out of the soil by rain and go into ground waters and nearby water-bodies (Ljung et al., 2009). Considering these adverse effects of acidic deposition in land ecosystems, serious impacts can be expected, especially in highly biodiverse and disturbance-sensitive forest ecosystems. The latter becomes much more likely if we add that emissions and related deposition in developing countries are rapidly increasing, and that 50–80 % of the fraction of deposition on land falls on natural vegetation and not close to the sources (Dentener et al., 2006).

Regarding the sources of deposition, SO_2 is emitted from different natural and anthropogenic processes. Volcanoes are considered the most important natural sources representing around 26–35 % of total global emissions (Graf et al., 1997; Stevenson et al., 2003). The most important anthropogenic sources are fossil fuel combustion from energy production, transportation, and industrial activity in big cities and their hinterlands, and biomass-burning from deforestation, land clearing, and bush fires (Lee et al., 2011; Smith et al., 2011). The contribution of each to the total SO_2 emissions may vary in accordance to the region and its development state (industrial or industrializing countries). However, in some tropical regions (e.g. Ecuador) volcanic emissions and biomass-burning might contribute to larger amounts in consequence of the density of active volcanoes (Carn et al., 2008) and an accelerated land use change mostly characterized by deforestation to gain arable land (Crutzen and Andreae, 1990; Rudel et al., 2005).

On a local to regional scale, detailed knowledge on pollutant deposition from rain and cloud water in specific regions, its sources, and its smaller-scale spatial variability, particularly in complex terrain as that of the Andes, is still scarce. To date, only few studies on atmospheric acidic deposition exist for tropical ecosystems and those including a characterization of source emissions are very rare.

Precipitation chemistry surveys in some montane but mainly lowland tropical forests of Costa Rica, Venezuela, Puerto Rico, Cameroon, and Brazil have characterized nutrient and pollutant deposition by analyzing ionic concentrations, among others sulfate, and in situ meteorological parameters. In Venezuela and Cameroon, Morales et al. (1998) and Sigha-Nkamdjou et al. (2003) indicated the relative importance of local sources, as biogenic sulfur oxidation by swamps and lakes, to sulfate depositions. However, industrial emissions were indicated as the most important source of sulfate deposition in Venezuela. The opposite was found by Eklund et al. (1997) and Gordon et al. (1994) in Costa Rica and Puerto Rico, respectively, where no significant pollution footprints where found in the samples of the two studied tropical mountain forests. The same was noticed by Pauliquevis et al. (2012) in the central Amazon of Brazil, where high sulfate loads in rain water likely stem from the oxidation of sulfur compounds from the Atlantic Ocean.

In areas with an important number of active volcanoes like Indonesia, Costa Rica, and Nicaragua, volcanic emissions were given a special attention as contributors of acidic sulfate deposition in the surrounding areas and downwind of the emitting craters (Delmelle et al., 2001, 2002; Langmann and Graf, 2003; Pfeffer et al., 2006). For Central Africa and tropical South America, however, emissions from burning forests, savannas, and agricultural fields were claimed as the principal source of atmospheric pollution (Hansen et al., 2013; Rissler et al., 2006; van der Werf et al., 2010) and reactive sulfur deposition in the downwind regions (Diehl et al., 2012; Fabian et al., 2005).

With regard to the megadiverse tropical mountain rainforest in the southeastern Ecuadorian Andes (Bendix and Beck, 2009), biomass-burning in the Amazon has been hitherto identified as the principal source of atmospheric sulfate deposition (Beiderwieden et al., 2005; Boy et al., 2008; Fabian et al., 2005, 2009; Rollenbeck et al., 2011). However, volcanic and biomass-burning emissions were included by roughly estimated data. Given the dense concecntration of active volcanoes in Ecuador, where as much as 95 % of emissions can stem from non eruptive degassing, and considering the difference in emissions between burned areas depending on land use type, it is of utmost importance to include data on source emissions as accurate as possible to characterize air-mass pollution history leading to the deposition. Furthermore, preliminary work on nitrogen deposition has shown that crest areas considerably differ in their behavior from valley sites (Makowski Giannoni et al., 2013). Hence, a comprehensive deposition analysis must not only investigate sinks and source intensities but should also study different topographic positions.

Consequently, the main aim of the current study is (1) to determine the sulfate deposition at two different topographic positions in the mountain rain forest of southern Ecuador and (2) to trace back the deposition to different natural and anthropogenic emission sources applying back trajectory modeling. To link the spatio-temporal patterns of upwind natural (volcanoes) and anthropogenic (urban/industrial and biomass-burning) sulfur emissions to sulfate deposition at site, we used the latest state of the art inventories and satellite data, also considering volcanic passive degassing.

ACPD
14, 13869–13908, 2014

2 Geographical setting

The Reserva Biológica San Francisco (RBSF) (4°00′ S and 79°00′ W) is located in a remote area at the outer edge of the Amazon, on the eastern slopes of the South Ecuadorian Andes, between the humid Amazon plains and the dryer interandean valleys. The RBSF lies within the small San Francisco River catchment between the capital cities of Loja and Zamora (Fig. 1). The forest and the anthropogenic replacement systems outside of the reserve have been subject of investigations from two successive multidisciplinary research groups funded by the German Research Council (DFG) since 2002 (Beck et al., 2008; Bendix et al., 2013). The terrain height of the area is lower compared to the northern and southern Andes and its topography more complex, as the system of few parallel mountain ranges gives way to a net of small valleys and cordilleras (Rollenbeck et al., 2011).

There are only few sources of pollution in the vicinity of the RBSF. The cities of Loja (∼ 214 855 inhabitants, 10 km to the west; INEC, 2010) and Zamora (∼ 25 510 inhabitants, 14 km south-east; INEC, 2010) are quite small and without any notable industrial activity. Between October and December, a relative dry season, slash and burn is a common practice in local pasture management which quite often runs out of control, burning adjacent areas of forest (Bendix et al., 2008b; Curatola Fernández et al., 2013; Hartig and Beck, 2003).

The synoptic winds at the upper levels of the cordillera consist of tropical easterly trades over more than 70 % of the time. North-easterlies prevail between January and March while south-easterlies dominate between June and September. The remaining 30 % corresponds to westerlies and northerlies, mainly occurring between end October and December (Bendix et al., 2008a; Emck, 2007).

Precipitation varies, mainly depending on the migration of the Inter Tropical Convergence Zone (ITCZ) and the variation in the direction of the tropical easterlies. The associated humidity advection dominates the amount of atmospheric water entering the ecosystem. The total annual average of rainfall (rainfall and occult precipitation)

ACPD
14, 13869–13908, 2014

range from 1850 to 6300 mm year-1 along an altitudinal gradient between 1960 and 3180 m a.s.l. Occult precipitation (OP) frequencies of up to 85 % of the time particularly occur in the more elevated parts of the research area, when warm and humid air masses from the Amazon lowlands hit the Andes, leading to intense condensation and clouds immersion (Bendix et al., 2006a, b; Emck, 2007; Rollenbeck, 2010).

3 Data and methods

In the present study we discuss the variation of sulfate deposition in precipitation in a five year period (2005–2009) at two MSs. Higher locations are more vulnerable to higher deposition (Makowski Giannoni et al., 2013), hence the selection of the two highest MSs in the RBSF for this study. We brought together long-term measurements of sulfate concentrations in rain and OP samples with backtrajectory transport modeling using satellite and emission inventories as inputs. The modeling of SO_2 transport, hereinafter referred to as "SO_2 transport", results in SO_2 daily concentration values at the target coordinates, which match the observation sites. Because of the strong winds at the locations of sampling, we will refer to all type of light precipitation, from wind-driven drizzle down to fog and cloud droplets as OP.

Sections 3.1 and 3.2 are devoted to a detailed description of the data and methods used to unveil the relationships between in-situ observations and transport until the observation sites.

3.1 Data

3.1.1 Sulfate deposition data

We measured rainfall and OP at two MSs: one installed on the highest surrounding peak (*Cerro del Consuelo*, 3180 m a.s.l.) and the other one on a mountain pass upriver (*El Tiro*, 2870 m a.s.l.), separating the basin of Loja in the west from the eastern slopes of the Andean mountain range (Fig. 1).

ACPD
14, 13869–13908, 2014

On the origin of atmospheric sulfate

S. Makowski Giannoni et al.

The collection of samples was conducted on a weekly basis between 2005 and 2009. Rain was sampled using UMS-RS 200 polyethylene rain samplers of 20 cm diameter. Standard fog collectors (Schemenauer and Cereceda, 1994) were used to sample OP. With a size of 1 m × 1 m and composed of polypropylene nets with a 2 mm × 1 mm mesh width, they were set up at 90° with respect to the main wind direction and collect all type of deposition, as particles, aerosols, and gases (Fabian et al., 2005). For further details on field measurement techniques, calibration, and handling of the data the reader is referred to Fabian et al. (2005) and Rollenbeck et al. (2007, 2011). On the day of collection, electrical conductivity (WTW-LF 90) and pH (Methron 73065/682) of the samples were measured on site. Then, the samples were stored deep frozen until chemical analyses were carried out.

Ion chromatography (Dionex DX-210) was used to measure concentrations of sulfate ions in rain and OP water. The sulfate ions were taken as proxies of sulfur inputs into the ecosystem. Finally, time series of sulfate volume weighted monthly mean (VWMM) concentrations and total deposition rates in rain and OP water were created for the period 2005–2009.

3.1.2 SO_2 source data

We used three recent emission inventories and one satellite dataset as emission inputs to simulate the SO_2 transport to our study area: (a) one for anthropogenic emissions (EDGARv4; Janssens-Maenhout et al., 2012), (b) one for biomass-burning (GFEDv3, Mu et al., 2011) and (c) one for emissions from volcanic degassing and explosive eruptions (Aerocom, Diehl et al., 2012). The ozone monitoring instrument (OMI) SO_2 data accounts mostly for SO_2 emissions from volcanoes, including passive degassing, but very strong anthropogenic pollution events are also detected by the sensor (Carn et al., 2007, 2008).

a. The emissions in EDGARv4 are calculated using a technology based emission factor approach which includes country-specific emissions when these are available. Emissions are allocated spatially on a $0.1^\circ \times 0.1^\circ$ grid cells for point, line, and area sources built upon geographic datasets such as the location of energy and manufacturing facilities, road networks, and population density. In version 4 EDGAR delivers now annual emission estimates from 1970 to 2008, which represents an advantage compared to former static inventories. For more information readers may visit the EDGAR website (http://edgar.jrc.ec.europa.eu/index.php).

b. For biomass-burning SO_2 estimates, we used the GFEDv3 inventory. The compilation of this inventory was based on a biogeochemical model (CASA-GFED) that approximates fuel loads and combustion completeness for each time-step, and burned area data from satellite observations (van der Werf et al., 2010). Considering that fires, as volcanic eruptions, are very often sporadic and transient, the high temporal and spatial resolution appear very advantageous when dealing with the variation of emissions in space and time. Some issues which might reduce the regional quality are the underestimation of emissions in the tropics because of cloud cover and canopy closeness, and gaps in the satellite coverage.

c. As part of the Aerocom global emission inventories, a daily-resolved volcanic SO_2 emission dataset was generated for the time period 1979–2009 including all volcanoes with historic eruptions listed in the Global Volcanism Program (http://www.volcano.si.edu/). Since volcanic emissions are in some cases occasional, the high temporal resolution of the inventory is indispensable for capturing the variability in the emission rates. Emissions for 1167 volcanoes considered to be active were compiled. The emissions originating from passive and quiescent degassing are also taken into account. The default SO_2 estimates are based on the Volcanic Sulfur Index (VSI). In cases where data from the total ozone mapping spectrometer (TOMS), OMI or the correlation spectrometer (COSPEC) were available the respective values were replaced by emissions calculated from these observations. In other cases the default values were replaced by more precise estimations from the literature. For more information on the Aerocom volcanic SO_2

inventory readers are referred to Diehl et al. (2012) and the Aerocom website (http://aerocom.met.no/emissions.html).

The OMI on board the polar-orbiting AURA satellite is a nadir solar backscatter spectrometer with a spatial footprint of 13 km × 24 km that spans the earth surface in one day. The instrument's UV-2 channel, which is used for the SO_2 retrievals, has a mean spectral resolution of 0.45 nm. Both, its spatial and spectral resolution, as well as its daily global coverage allows for a SO_2 retrieval based monitoring of low emission sources like volcanic passive degassing and smelter plumes which was not possible with former instruments like TOMS or GOME. OMI SO_2 data was already successfully applied for daily monitoring of volcanic degassing in Ecuador (Carn et al., 2008) and the detection of SO_2 emissions from Peruvian copper smelters (Carn et al., 2007). Although the OMI instrument cannot distinguish between anthropogenic and volcanic SO_2 when co-occurring in close vicinity, Carn et al. (2007) concluded that anthropogenic sources in the coastal plains of Ecuador would only contribute to less than 1 % to the total amount measured by OMI. In the current study, we used subsets of the OMI data replicating the same geographical domain defined by Carn et al. (2008) for Ecuadorian volcanic emissions. The region selected is not affected by the South-Atlantic anomaly, an artifact impacting on the retrievals of a big area in central and southern South America (Lee et al., 2011), which means that OMI retrievals are reliable in the selected domain. The concentration retrieved by OMI was assumed to represent mainly the Ecuadorian volcanic emission's contribution to the atmospheric SO_2 concentrations. Given its small geographic domain, the OMI data is set to account for regional emissions from Ecuador and southern Colombia.

3.2 Methods

3.2.1 Trajectory modeling

To link potential SO_2 source regions with the deposition in our study site, a tool was developed which models the transport of SO_2 from upwind sources (biomass-burning, anthropogenic, and volcanic emissions) to our receptor area. The tool follows the path of the trajectories and adds the emission amounts from the pixels that prove spatial and temporal coincidence until a target point which corresponds to the coordinates of the RBSF. No chemical or physical transformations are included in the modeling scheme. Scavenging and rain-out processes are accounted for by a decay function integrated into the algorithm. For more details on the tool refer to Rollenbeck (2010) and Makowski Giannoni et al. (2013).

3.2.2 Observation and model data processing and evaluation

To calculate best estimates of precipitation (rain and OP), we used a method similar to the one used in the Goddard Institute for Space Studies Surface Temperature Analysis (GISTEMP, Hansen et al., 2010). Nearby MSs were used to evaluate unrealistic values and to fill-in data gaps of the MSs that we used in this study.

Conductivity and pH time-series of VWMM were compiled and summary statistics as median, median absolute deviation (MAD), and minimum and maximum values calculated. These values were then compared to those in the sulfate concentration time-series to check for acidification of the samples when highly loaded with sulfate ions.

As mentioned in the last paragraph, we compiled sulfate VWMM concentrations into time-series covering the whole observation period, where we looked for the time span in which peak values or regular phenomena took place, as well as long term trends.

The daily transport model outputs were first aggregated according to the dates of sample collection in the field, in order to achieve comparable values for time-series compilation and correlation analysis. We calculated the mean weekly values to compensate for irregular time intervals between collection of samples. We then used these new values to calculate SO_2 transport monthly averages and to compile transport time-series from the different emission sources represented by the emission inventories and satellite data.

We calculated and analyzed annual mean deposition rates for *El Tiro* and *Cerro del Consuelo* MSs. Then, we carried out a Pearson correlation analysis to test for correlations between field observations (sulfate concentrations) and model outputs (SO_2 transport); we used VWMM and not deposition values to avoid extra uncertainty added by new variables present in the deposition calculations. Finally, visual analysis of coincidences between transport and VWMM concentration time-series was performed, taking into account events which could influence the transport of sulfate and its deposition into our study area. Before proceeding with statistical analysis, the data was transformed to a logarithmic scale to approach normality.

In addition to the bivariate correlation analysis, we applied a factor analysis with varimax rotation to test for variance explanation from groups of variables.

4 Results

4.1 Emission sources and annual deposition

The highest water inputs were registered from April to July at *Cerro del Consuelo* MS (Fig. 2a), and in February and from April to June, at *El Tiro* MS (Fig. 2b). A short dry season took place between September and November. Rain quantity varied significantly between dry and wet periods while OP inputs remained quite constant around 100 mm for both MSs over the whole observation period.

The calculated volume-weighted monthly pH values in samples from *Cerro del Consuelo* MS yielded median values of 5.3 and 5 with a MAD of 0.36 and 0.29 in rain and OP, respectively (Table 1). The water samples in both types of water inputs tended to be acidic with some extreme values going as low as 1.86 in OP samples and 3 in rain samples. OP sulfate concentration presented a negative, weak but significant correlation with pH values (Pearson, $r = -0.34$, $p < 0.05$). Conductivity values ranged between 1.4 and 72 $\mathrm{S\,m^{-1}}$, with median values of 2.6 and 8.1 $\mathrm{S\,m^{-1}}$ in OP and rain, respectively. The bulk of the data ranged, nevertheless, between 1.4 and 14.3 $\mathrm{S\,m^{-1}}$. Conductivity is a proxy of ion concentrations in water and thus, high conductivity values coincide with episodes of highly loaded rain and OP water droplets.

In samples from *El Tiro* MS, pH volume-weighted values were in the acidic area of the spectrum too, with median values of 5.4 and 4.8 and MAD of 0.51 and 0.37 in rain and OP, respectively (Table 1). There was a strong negative correlation between sulfate concentration in OP and pH (Pearson, $r = -0.64$, $p < 0.001$), and a weaker one for sulfate concentration in rain (Pearson, $r = -0.34$, $p < 0.05$). Median conductivity values were generally higher compared to those at *Cerro del Consuelo* MS. They yielded a median of 10.9 and 3.7 $\mathrm{S\,m^{-1}}$ in OP and rain, respectively. Opposed to what we observed at *Cerro del Consuelo* MS, conductivity was much higher in OP than in rain at *El Tiro* MS, meaning a strong ion load; values ranged between 1.4 and 110.3 $\mathrm{S\,m^{-1}}$.

Figure 3 shows the annual sulfate deposition by rain and OP at (a) *Cerro del Consuelo* and (b) *El Tiro* MSs. The deposition was generally higher for *Cerro del Consuelo* MS for both types of precipitation. The only exception was the year 2009 where the OP deposition at *El Tiro* MS increased significantly in comparison to a decrease at *Cerro del Consuelo*. The highest amount of sulfate was deposited by rain in 2007 at the *Cerro del Consuelo* MS. Lowest burden was observed in rain samples from *El Tiro* MS in 2009. The figure shows that *El Tiro* MS was experiencing higher annual deposition rates by OP nearly over all years, pointing to a more advective environment. In contrary, *Cerro del Consuelo* MS was characterized by changing deposition maxima between rain and OP over time.

A tendency towards lower OP sulfate deposition (light gray bars) was observed in Fig. 3, with an upturn in 2009 for *El Tiro* MS. Deposition by rain (dark gray bars) was more oscillating, especially in the quantities deposited at *Cerro del Consuelo* MS. At the latter MS, an evident decrease in rain deposition started in 2008 after an abrupt increase in 2007. Strikingly, that year the deposition also began to be dominated by this type of precipitation.

Concerning the emisssions, Fig. 4 depicts five year average maps of emissions for every dataset used for simulating transport. From a rather local perspective, emissions from volcanoes appeared to be intense mainly close to the most active volcanoes: *Sangay*, *Tungurahua* and *Reventador* (Fig. 4a). Emissions form big cities only seemed to be evident for the metropolitan region of Guayaquil and Quito, but much seems contaminated with SO_2 emissions from volcanoes, which plumes were transported principally to the west and south west and cover part of the ocean next to the southern coast of the country. The strong emissions east of *Reventador* most probably have its origin in deforestation activity. The high emission pixels at the same location in the biomass-burning dataset (Fig. 4c) support this argument.

Figure 4b show volcanic emissions from eruptions and passive degassing. Once again, *Sangay*, *Tungurahua*, and *Reventador* belong to the volcanoes that contribute the most to the emissions in Ecuador. In Colombia, *Nevado del Huila* and *Galeras* are the strongest SO_2 emitters. For biomass-burning, the main region is located in the Brazilian and Bolivian Amazon (Fig. 4c). The Venezuelan savanna in the north-east is another important biomass-burning region. The majority of potential anthropogenic sources (industrial, urban, and transportation) are located in the north of our study area (Fig. 4d). This occurs owing to the extremely scarce significant sources in the east and because no air masses arriving to our study area originate and overpass the potential sources in the south.

4.2 Linking emissions to deposition

4.2.1 Correlation analyses

A first test, using cross-correlation technique, is required to unveil the dependence of the transport data sets. This is shown in Table 2. Only moderate relations for *El Tiro* and somewhat higher correlations for *Cerro del Consuelo* were revealed by this analysis.

As expected, volcanic and anthropogenic source concentrations correlate well while only low (partly negative) correlations between biomass-burning and anthropogenic and volcanic pollutant transport is visible. This means that there is some overlap in the data sets related to volcanic and anthropogenic emissions. The negative correlation between anthropogenic and biomass-burning could indicate that their transport depends on changing wind direction (east for biomass-burning, north and west for anthropogenic) which means that the anthropogenic sources affecting the area are located more in the western and northern sectors.

To connect sinks with sources, correlation analysis between atmospheric SO_2 concentration in the pixel representing the location of the observation site, derived by back-trajectory modeling, and the measured sulfate deposition was conducted. Pearson's correlation coefficients calculated for sulfate concentration and SO_2 transport are presented in Table 3. It could be observed that, even if significant, the correlations between source and sink data are generally low.

For *Cerro del Consuelo* crest site it is interesting to see that more evident correlations occur between OP and volcanic emissions. Because OMI includes volcanic emissions, it shows the second highest correlation coefficient for OP. The link to biomass-burning seems to be generally weak at these altitude and topographical location of the cordillera.

The situation changes for the *El Tiro* up-valley MS, where the highest correlations occur between rain deposition and anthropogenic sources and between OP deposition and biomass-burning sources.

Even if the correlation coefficients are low, they show interesting tendencies. For *El Tiro* site, volcanic and anthropogenic emissions are more clearly related to rain deposition while the opposite is true for biomass-burning, which is more strongly related to OP deposition. OMI shows a mixed behavior because it includes volcanic as well as regional anthropogenic emissions as shown in Table 2 and Fig. 4.

Rather low correlation coefficients mean that no unique source can totally explain the oscillations in the deposition. Furthermore, correlation coefficients are blurred because

ACPD
14, 13869–13908, 2014

peaks are extreme values, which represent scatter. The concentration time-series are a sum curve of all transport values. By exploring time-series of sink and transport from sources, the next subsection (Sect. 4.2.2) sheds some light on what groups of transport variables explain the most of the variability in the concentration variables.

4.2.2 Analysis of monthly time-series

Figure 5 shows the time series of SO_2 transport (concentrations at the pixels above the study site) and the respective sulfate concentrations observed at the sites. We observed that mainly depending on emission state and airmass history, emission peaks resulted in deposition peaks of different intensity. One general finding is that the peak concentrations in biomass-burning transport were ~ 56 times higher than those of the other sources. Besides, there was a slight tendency for increasing emissions from anthropogenic, regional and even volcanic sources in the observation period. At the same time, emissions due to biomass-burning decreased, particularly in the last years of the study period (2008, 2009) which is consistent with deforestation statistics in Brazil (Hansen et al., 2013; Rodrigues-Ramos et al., 2011; Torres et al., 2010).

Regarding relations between wind direction and the link between sources and sinks it is obvious that during easterly airstream coinciding with the Amazon biomass-burning season from August to October (light gray bars) (Andreae et al., 2004), biomass emission peaks caused deposition peaks. On the contrary, during wind directions from the northern and western sector (dark grey), peaks in volcanic activity and anthropogenic emissions in central/northern Ecuador could be clearly related to deposition peaks.

El Tiro MS had higher sulfate loads in fog than in rain. A decrease following the reduction in biomass-burning was observed in the OP sulfate concentration time-series from 2007 to 2008 with a violent upturn at the end of the biomass-burning season of 2009 (Fig. 5a) for which we have not found any explanation yet; this last peak is responsible for the light positive tendency of the curve. Rain sulfate time-series (Fig. 5b) presented a light negative tendency over the observed period (2005–2009).

In OP, only one peak in the biomass-burning time-series (July 2008) seemed to dominate the deposition. Volcanic transport did not play a role. In rain, biomass-burning and volcanic transport peaks were both reflected in the deposition time series, with a stronger coincidence with volcanic emissions. Anthropogenic sources showed the same peak coincidences with rain water sulfate concentrations during northerly winds (particularly in 2005 and 2008). However, volcanic transport was quantitatively higher than that from anthropogenic sources, which means that it likely contributed more to the deposition.

At the uppermost and more exposed *Cerro del Consuelo* MS we observe a different situation, namely a very light negative tendency in the sulfate concentrations in both OP (Fig. 5a) and rain (Fig. 5b). OP sulfate concentrations are also here higher than in rain. In this case, the negative trend of the biomass-burning SO_2 transport with the highest transport (Fig. 5e) seems to dominate the deposition's temporal development irrespective of the type or precipitation. Biomass-burning peaks are affecting only rain deposition, except for one emission peak in August 2005, which is affecting both OP and rain deposition (this is more or less the same for *El Tiro* MS). Interestingly, volcanic transport peaks (Fig. 5d) are mostly affecting OP concentrations. This is definitely different from *El Tiro* MS, where no influence in OP concentrations was noticed. EDGAR anthropogenic transport (Fig. 5f) is nonetheless also reflected in OP concentrations, but again here the transport was quantitatively lower.

Between March and May 2005–2007 a small peak in the biomass-burning SO_2 transport time-series can be seen, which very likely corresponds to the emissions of the Venezuelan savanna's biomass-burning season as observed by Hamburger et al. (2013). Apparently, this biomass-burning emission source has no significant resonance in the deposition at our study site. In 2008 and 2009 the peaks almost disappear, again coinciding with the anomalous biomass-burning season these two years (Torres et al., 2010).

ACPD
14, 13869–13908, 2014

4.2.3 Factor analysis

Table 4 presents the results from factor analysis applied to observational and modeled data. A main outcome is that the three first factors explain more than 80 % of the variance for both *El Tiro* and *Cerro del Consuelo* MSs.

For *Cerro del Consuelo* MS, the eigenvectors show that biomass-burning SO_2 transport (GFED) was related to the sulfate deposition in rain, since both loaded to the factors 2 and 3. The rest was more closely related to sulfate deposition in OP, with loadings to factors 2, 4 and 5. The communalities also show that factor 2 was dominated by biomass-burning SO_2 (GFED) and rain sulfate deposition. Factor 1 shows important loadings of OP sulfate deposition and SO_2 transport from all other source datasets (OMI, Aerocom, and EDGAR).

At *El Tiro* MS, the relationship was inverse; biomass-burning SO_2 modeled transport and OP SO_2 deposition were more closely related, both of them contributing to factor 2. Loadings from rain sulfate deposition and all other source dataset contributed to factor 1, and therefore they lied close in the multidimensional space. This is stressed by the communalities, where both the variance of OP sulfate deposition and biomass-burning SO_2 transport contributed mainly to factor 2, and rain sulfate deposition and the SO_2 transport from the rest of emission sources to factor 1.

5 Discussion

In this study, we concerned ourselves with the identification of important natural and anthropogenic sources contributing to atmospheric sulfate deposition in the tropical mountain forests of southeastern Ecuador. Special attention was given to the contribution of natural volcanic emissions, given that the study site is located in a region with a very high density of active volcanoes (Carn et al., 2008).

Based on fire pixels, emission inventories, and back-trajectories several previous studies (Fabian et al., 2005, 2009; Rollenbeck, 2010; Rollenbeck et al., 2006) pin

ACPD
14, 13869–13908, 2014

pointed biomass-burning as the principal source of atmospheric sulfate. These did not use, however, neither data on explosive emissions nor passive degassing, which represents a considerable part of the total volcanic emissions (Carn et al., 2008). Because of the latter argument, we came to the idea that the contribution of volcanoes to the sulfate deposition in the area could have being underestimated.

Contrary to what we expected, we found that, quantitatively, volcanic emission sources did no play a major role, even if they were more important than anthropogenic emissions. Biomass-burning sources were indeed dominant substantially for two reasons: first, because easterlies are strong and constant, which is translated in preponderant airmass-transport from the east (Bendix et al., 2008b), where the main biomass-burning region is located; second, because biomass-burning emissions in the Brazilian Amazon are strong and the area burned covers a very large surface (Giglio et al., 2010; Prins and Menzel, 1992), making it more likely for the emissions to be advected. Transport from the north and west occured only for short periods and the sources of SO_2 did not cover such a big surface as biomass-burning in the Brazilian Amazon did (Fig. 4c). However, no single emission sources explained the variability in the deposition but a sum of single contributions, always depending on the type of precipitation and the topographic features of the site where samples where gathered.

The correlation analysis between SO_2 transport and sulfate concentrations resulted in some significant but not so strong correlations. Furthermore, the comparison of time-series revealed that no single transport curve completely matches neither OP nor rain concentrations. The different source-related transport curves coincided only in specific time-periods with the concentration curves, producing deposition in OP and/or rain depending on the location of the MS. This is clarified in the following subsections (Sect. 5.1 and 5.2) and a graphical interpretation is given in Fig. 6.

5.1 Easterly transport

The correlation between *El Tiro* MS and biomass-burning transport was significant but weak only for OP samples. This relationship was supported by factor analysis.

ACPD
14, 13869–13908, 2014

In the period from August to October, the tropical easterlies still blow strongly and persistently and overlap with the occurrence of the biomass-burning season in the Amazon basin. Sulfur emissions, basically from the Brazilian Amazon, are transported towards the west until they encounter the first foothills and cordilleras of the Andean mountain range, where intense scavenging of pollutants takes place. The connection to the emissions in the Amazon basin is mainly noticed in OP sulfate concentrations from *El Tiro* MS (dark grey bars in Fig. 5a and e). Here concentration peaks coincide with SO_2 transport. Biomass-burning has a mean low injection height into the atmosphere (max. 3 km, but only a very thin haze, while the main heating at 850 hPa represents a mean injection height of 1.5 km, Davidi et al., 2009) which means that the pollution is transported in the lower valley upwards with the upvalley winds and hit the fog collectors at *El Tiro* (2660 m a.s.l.).

The same easterly air-masses hit the mountain on which top *Cerro del Consuelo* MS is located, and are adiabatically uplifted producing intense rainfall and OP mainly windward but also on the summit. The fog collector is not located directly on the windward hillside, exposed to ascending airmasses, so the ion loaded water is apparently mostly collected by the rain gauges, as shown by time-series and factor analysis. However, measurements from fog collectors and rain gauges overlap here more frequently than at *El Tiro*, making the separation between rain and OP more difficult. The result is that rain and OP differentiation is fuzzy, which is blurring the correlations between concentrations and transport. Hence, the biomass-burning signal is here relatively low.

5.2 Northerly and westerly transport

Volcanic and anthropogenic transport were significantly correlated to sulfate concentrations from *El Tiro* MS rain samples and OP samples from *Cerro del Consuelo* MS. The same was also reflected in the results of the factor analysis.

Between October and January, as northerlies set in, the volcanic SO_2 transport time-series coincide with those of sulfate concentrations from the MSs, especially regarding sulfate in rain, from *El Tiro* MS, and in OP from *Cerro del Consuelo* MS. The greater

ACPD
14, 13869–13908, 2014

recurrence of coincidences with the rain time-series at *El Tiro* MS is explained by its location at a mountain pass which links the eastern slopes and the interandean valley of Loja. The two parallel east-to-west mountain ranges mark the boundaries of the San Francisco Valley. As already mentioned (Sect. 5.1), they shape the wind field, favoring the advected polluted air-masses coming from the east or west, like biomass-burning transport, to impact the vegetation and the east-west oriented fog collectors on the mountain pass. Clouds advected from the north and north-west (likely charged with SO_2 ions) are partially blocked by the delimiting mountain range at the north. Hence, only rain gauges can collect sulfate scavenged from these clouds as rain drops traverse the atmosphere on their way to the ground.

Between 20 % and 50 % of wind trajectories reach the RBSF from the north, over-passing areas of active volcanoes. Volcanoes in the Andes lie at altitudes that in most of the cases exceed the 4000 m a.s.l., so even emissions from degassing can contaminate high clouds in the lower troposphere (Diehl et al., 2012; Stuefer et al., 2012). These months there is also an increment in the transport of anthropogenic SO_2, most likely in response to the air masses passing over emission sources from Ecuadorian and maybe Colombian cities. Anthropogenic sources in the Andes north of the RBSF also lie at high altitudes and, as recent studies reported for Europe, this type of emissions can also reach higher atmospheric levels as previously assumed (Bieser et al., 2011). The latter would make anthropogenic plumes from Ecuadorian big cities in the Andes prone to reach higher clouds in the atmosphere as well. Therefore, northerly air-masses charged with volcanic sulfate particles, and to a lesser extent anthropogenic, directly impinges the mountain where *Cerro del Consuelo* fog collector is located on the windward (north facing slopes) side. OP water is here a major part of precipitation (41 % of rainfall; Bendix et al., 2008a, b). In addition, it is located at 3200 m a.s.l., probably more exposed to pollutants transported through higher atmospheric levels than at *El Tiro* MS. Multicollinearity found between volcanic, anthropogenic, and regional (Ecuadorian) transport datasets reinforces this hypothesis (Table 2).

6 Conclusions

We conclude that biomass-burning sources are dominating the sulfate deposition as a result of strong and persistent easterly sulfate transport of emissions from wide burned areas of Amazon forests and its anthropogenic replacement systems. These take place during the main Amazon biomass-burning season between August and October. Between October and December, the main wind direction shifts to the north and west, transporting volcanic and anthropogenic sulfate to our study site. The transport from these sources is, nonetheless, much inferior compared to biomass-burning.

We found two different deposition regimes at the evaluated topographic sites. The up-valley mountain pass *El Tiro*, is located on the eastern side of the ridge and is characterized by a more advective environment with dominating OP deposition from low tropospheric fire-polluted air-masses from the Amazon lowlands. Sulfate from volcanic and anthropogenic emissions are episodically transported through a higher atmospheric level from the north and, as there is no cloud immersion during this wind directions, sulfate can be only deposited by rain.

At the highest mountain crest of the study area, *Cerro del Consuelo*, the situation is less homogeneous and less clear. Deposition was dominated by OP until 2007, when it started to be dominated by rain. Sulfate deposition by OP is likely linked to volcanic and anthropogenic sources in the north, as a consequence of its higher location and its orientation. The higher atmospheric transport reaches *Cerro del Consuelo* MS from all wind directions and thus contaminate the cloud fog resulting in OP deposition. According to the cross-correlation results, biomass-burning has no significant relation to this site's deposition. Overlapping of rain gauge and fog collector measurements made the differentiation of deposition types difficult. However, time-series and factor analyses show a likely contribution of human induced fires in the lowlands to sulfate deposition by rain at *Cerro del Consuelo* MS. The higher conductivity of the rain samples point to the likely higher contamination of the rain samples as well.

ACPD
14, 13869–13908, 2014

In general, this study revealed that even if volcanic emission are proximate and numerous, they do not dominate the sulfate deposition at the RBSF. The shape and size of the sources, as well as the consistency of the winds are important parameters that determined the dominance of biomass-burning in the deposition at the study site. However, the importance of topography has also been stressed as important parameter conditioning the type and quantity of deposition in areas with complex terrain.

Author contribution

J. B., R. R., and S. M. G. designed the experiments and S. M. G. carried them out. R. R. developed the trajectory model code and S. M. G. performed the simulations. S. M. G. and K. T. collected, processed, and adapted the satellite data and emission inventories to the format requested for model runs. S. M. G. analyzed the data and prepared the manuscript with contributions from all co-authors.

Acknowledgements. We thank the German Academic Exchange Service (DAAD) for funding the PhD thesis of Sandro Makowski Giannoni (Ref. Number A/08/98222) and the German Research Foundation (DFG) for the funding of the work in the scope of the Research Unit RU816 (funding number: BE 1780/15-1). We are grateful to Lukas Lehnert, Nicolas Caspari, and Maik Dobermann for their valuable help. We also thank the foundation Nature & Culture International (NCI) Loja and San Diego for logistic support. We finally thank Giulia F. Curatola Fernández for proof reading.

References

Andreae, M. O., Rosenfeld, D., Artaxo, P., Costa, A. A., Frank, G. P., Longo, K. M., and Silva-Dias, M. A. F.: Smoking rain clouds over the Amazon, Science, 303, 1337–1342, doi:10.1126/science.1092779, 2004.

Beck, E., Bendix, J., Kottke, I., Makeschin, F., and Mosandl, R. (Eds.): Gradients in a Tropical Mountain Ecosystem of Ecuador, Springer Berlin/Heidelberg, Berlin, Germany, 2008.

Beiderwieden, E., Wrzesinsky, T., and Klemm, O.: Chemical characterization of fog and rain water collected at the eastern Andes cordillera, Hydrol. Earth Syst. Sci., 9, 185–191, doi:10.5194/hess-9-185-2005, 2005.

Bendix, J. and Beck, E.: Spatial aspects of ecosystem research in a biodiversity hot spot of southern Ecuador – an introduction, Erdkunde, 63, 305–308, doi:10.3112/erdkunde.2009.04.01, 2009.

Bendix, J., Rollenbeck, R., Göttlicher, D., and Cermak, J.: Cloud occurrence and cloud properties in Ecuador, Clim. Res., 30, 133–147, doi:10.3354/cr030133, 2006a.

Bendix, J., Rollenbeck, R., and Reudenbach, C.: Diurnal patterns of rainfall in a tropical Andean valley of southern Ecuador as seen by a vertically pointing K-band Doppler radar, Int. J. Climatol., 26, 829–846, doi:10.1002/joc.1267, 2006b.

Bendix, J., Rollenbeck, R., Göttlicher, D., Nauß, T., and Fabian, P.: Seasonality and diurnal pattern of very low clouds in a deeply incised valley of the eastern tropical Andes (South Ecuador) as observed by a cost-effective WebCam system, Meteorol. Appl., 15, 281–291, doi:10.1002/met.72, 2008a.

Bendix, J., Rollenbeck, R., Richter, M., Fabian, P., and Emck, P.: Climate, in: Gradients in a Tropical Mountain Ecosystem of Ecuador, edited by: Beck, E., Bendix, J., Kottke, I., Makeschin, F., and Mosandl, R., Springer Berlin/Heidelberg, 63–74, available at: doi:10.1007/978-3-540-73526-7_8, 2008b.

Bendix, J., Beck, E., Bräuning, A., Makeschin, F., Mosandl, R., Scheu, S., and Wilcke, W. (Eds.): Ecosystem Services, Biodiversity and Environmental Change in a Tropical Mountain Ecosystem of South Ecuador, Springer Berlin/Heidelberg, Berlin, Germany, 2013.

Bieser, J., Aulinger, A., Matthias, V., Quante, M., and Denier van der Gon, H. A. C.: Vertical emission profiles for Europe based on plume rise calculations, Environ. Pollut., 159, 2935–2946, doi:10.1016/j.envpol.2011.04.030, 2011.

Boy, J., Rollenbeck, R., Valarezo, C., and Wilcke, W.: Amazonian biomass burning-derived acid and nutrient deposition in the north Andean montane forest of Ecuador, Global Biogeochem. Cy., 22, GB4011, doi:10.1029/2007GB003158, 2008.

Carn, S. A., Krotkov, N. A., Yang, K., Hoff, R. M., Prata, A. J., Krueger, A. J., Loughlin, S. C., and Levelt, P. F.: Extended observations of volcanic SO_2 and sulfate aerosol in the stratosphere, Atmos. Chem. Phys. Discuss., 7, 2857–2871, doi:10.5194/acpd-7-2857-2007, 2007.

Carn, S. A., Krueger, A. J., Arellano, S., Krotkov, N. A., and Yang, K.: Daily monitoring of Ecuadorian volcanic degassing from space, J. Volcanol. Geoth. Res., 176, 141–150, doi:10.1016/j.jvolgeores.2008.01.029, 2008.

Crutzen, P. J. and Andreae, M. O.: Biomass burning in the tropics: impact on atmospheric chemistry and biogeochemical cycles, Science, 250, 1669–1678, doi:10.1126/science.250.4988.1669, 1990.

Curatola Fernández, G. F., Silva, B., Gawlik, J., Thies, B., and Bendix, J.: Bracken fern frond status classification in the Andes of southern Ecuador: combining multi-spectral satellite data and field spectroscopy, Int. J. Remote Sens., 34, 7020–7037, doi:10.1080/01431161.2013.813091, 2013.

Davidi, A., Koren, I., and Remer, L.: Direct measurements of the effect of biomass burning over the Amazon on the atmospheric temperature profile, Atmos. Chem. Phys., 9, 8211–8221, doi:10.5194/acp-9-8211-2009, 2009.

Delmelle, P., Stix, J., Bourque, C. P.-A., Baxter, P. J., Garcia-Alvarez, J., and Barquero, J.: Dry deposition and heavy acid loading in the vicinity of Masaya Volcano, a major sulfur and chlorine source in Nicaragua, Environ. Sci. Technol., 35, 1289–1293, doi:10.1021/es000153m, 2001.

Delmelle, P., Stix, J., Baxter, P. J., Garcia-Alvarez, J., and Barquero, J.: Atmospheric dispersion, environmental effects and potential health hazard associated with the low-altitude gas plume of Masaya volcano, Nicaragua, B. Volcanol., 64, 423–434, doi:10.1007/s00445-002-0221-6, 2002.

Dentener, F., Drevet, J., Lamarque, J. F., Bey, I., Eickhout, B., Fiore, A. M., Hauglustaine, D., Horowitz, L. W., Krol, M., Kulshrestha, U. C., Lawrence, M., Galy-Lacaux, C., Rast, S., Shindell, D., Stevenson, D., Van Noije, T., Atherton, C., Bell, N., Bergman, D., Butler, T., Cofala, J., Collins, B., Doherty, R., Ellingsen, K., Galloway, J., Gauss, M., Montanaro, V., Müller, J. F., Pitari, G., Rodriguez, J., Sanderson, M., Solmon, F., Strahan, S., Schultz, M., Sudo, K., Szopa, S., and Wild, O.: Nitrogen and sulfur deposition on regional and global scales: a multi-model evaluation, Global Biogeochem. Cy., 20, GB4003, doi:10.1029/2005GB002672, 2006.

Diehl, T., Heil, A., Chin, M., Pan, X., Streets, D., Schultz, M., and Kinne, S.: Anthropogenic, biomass burning, and volcanic emissions of black carbon, organic carbon, and SO_2 from 1980 to 2010 for hindcast model experiments, Atmos. Chem. Phys. Discuss., 12, 24895–24954, doi:10.5194/acpd-12-24895-2012, 2012.

ACPD
14, 13869–13908, 2014

S. Makowski Giannoni et al.

Eklund, T., McDowell, W., and Pringle, C.: Seasonal variation of tropical precipitation chemistry: La Selva, Costa Rica, Atmos. Environ., 31, 3903–3910, available at: http://www.sciencedirect.com/science/article/pii/S135223109700246X (last access: 20 February 2014), 1997.

Elser, J. J., Bracken, M. E. S., Cleland, E. E., Gruner, D. S., Harpole, W. S., Hillebrand, H., Ngai, J. T., Seabloom, E. W., Shurin, J. B., and Smith, J. E.: Global analysis of nitrogen and phosphorus limitation of primary producers in freshwater, marine and terrestrial ecosystems, Ecol. Lett., 10, 1135–1142, doi:10.1111/j.1461-0248.2007.01113.x, 2007.

Emck, P.: A climatology of South Ecuador, University of Erlangen, available at: http://www.opus.ub.uni-erlangen.de/opus/volltexte/2007/656/ (last access: 15 August 2012), 2007.

Fabian, P., Kohlpaintner, M., and Rollenbeck, R.: Biomass burning in the Amazon-fertilizer for the mountaineous rain forest in Ecuador, Environ. Sci. Pollut. R., 12, 290–296, doi:10.1065/espr2005.07.272, 2005.

Fabian, P., Rollenbeck, R., Spichtinger, N., Brothers, L., Dominguez, G., and Thiemens, M.: Sahara dust, ocean spray, volcanoes, biomass burning: pathways of nutrients into Andean rainforests, Adv. Geosci., 22, 85–94, doi:10.5194/adgeo-22-85-2009, 2009.

Giglio, L., Randerson, J. T., van der Werf, G. R., Kasibhatla, P. S., Collatz, G. J., Morton, D. C., and DeFries, R. S.: Assessing variability and long-term trends in burned area by merging multiple satellite fire products, Biogeosciences, 7, 1171–1186, doi:10.5194/bg-7-1171-2010, 2010.

Gordon, C., Herrera, R., and Hutchinson, T.: Studies of fog events at two cloud forests near Caracas, Venezuela – II. Chemistry of fog, Atmos. Environ., 28, 323–337, available at: http://www.sciencedirect.com/science/article/pii/1352231094901082 (last access: 23 May 2012), 1994.

Graf, H.-F., Feichter, J., and Langmann, B.: Volcanic sulfur emissions: estimates of source strength and its contribution to the global sulfate distribution, J. Geophys. Res., 102, 10727, doi:10.1029/96JD03265, 1997.

Greaver, T. L., Sullivan, T. J., Herrick, J. D., Barber, M. C., Baron, J. S., Cosby, B. J., Deerhake, M. E., Dennis, R. L., Dubois, J.-J. B., Goodale, C. L., Herlihy, A. T., Lawrence, G. B., Liu, L., Lynch, J. A., and Novak, K. J.: Ecological effects of nitrogen and sulfur air pollution in the US: what do we know?, Front. Ecol. Environ., 10, 365–372, doi:10.1890/110049, 2012.

Hamburger, T., Matisāns, M., Tunved, P., Ström, J., Calderon, S., Hoffmann, P., Hochschild, G., Gross, J., Schmeissner, T., Wiedensohler, A., and Krejci, R.: Long-term in situ observations

of biomass burning aerosol at a high altitude station in Venezuela – sources, impacts and interannual variability, Atmos. Chem. Phys., 13, 9837–9853, doi:10.5194/acp-13-9837-2013, 2013.
Hansen, J., Ruedy, R., Sato, M., and Lo, K.: Global surface temperature change, Rev. Geophys., 48, RG4004, doi:10.1029/2010RG000345, 2010.
Hansen, M. C., Potapov, P. V, Moore, R., Hancher, M., Turubanova, S. A., Tyukavina, A., Thau, D., Stehman, S. V, Goetz, S. J., Loveland, T. R., Kommareddy, A., Egorov, A., Chini, L., Justice, C. O., and Townshend, J. R. G.: High-resolution global maps of 21st-century forest cover change, Science, 342, 850–853, doi:10.1126/science.1244693, 2013.
Hartig, K. and Beck, E.: The bracken fern (*Pteridium arachnoideum* (Kaulf.) Maxon) dilemma in the Andes of Southern Ecuador, Ecotropica, 9, 3–13, 2003.
Instituto Nacional de Estadística y Censos (INEC): Fascículo provincial Zamora Chinchipe, Result. del censo población y vivienda, available at: http://www.ecuadorencifras.gob.ec/wp-content/descargas/Manu-lateral/Resultados-provinciales/ (last access: 23 May 2014), 2010.
Janssens-Maenhout, G., Dentener, F., Aardenne, J. van, Monni, S., Pagliari, V., Orlandini, L., Klimont, Z., Kurokawa, J., Akimoto, H., Ohara, T., Wankmüller, R., Battye, B., Grano, D., Zuber, A., and Keating, T.: EDGAR-HTAP: a harmonized gridded air pollution emission dataset based on national inventories, scientific report, Joint Research Center, European Comision, 41 pp., Ispra, Italy, 2012.
Kuylenstierna, J. C. I., Rodhe, H., Cinderby, S., and Hicks, K.: Acidification in developing countries: ecosystem sensitivity and the critical load approach on a global scale, AMBIO, 30, 20–28, doi:10.1579/0044-7447-30.1.20, 2001.
Langmann, B. and Graf, H. F.: Indonesian smoke aerosols from peat fires and the contribution from volcanic sulfur emissions, Geophys. Res. Lett., 30, 1547, doi:10.1029/2002GL016646, 2003.
Lee, C., Martin, R. V, van Donkelaar, A., Lee, H., Dickerson, R. R., Hains, J. C., Krotkov, N., Richter, A., Vinnikov, K., and Schwab, J. J.: SO_2 emissions and lifetimes: estimates from inverse modeling using in situ and global, space-based (SCIAMACHY and OMI) observations, J. Geophys. Res., 116, D06304, doi:10.1029/2010JD014758, 2011.
Ljung, K., Maley, F., Cook, A., and Weinstein, P.: Acid sulfate soils and human health – a millennium ecosystem assessment, Environ. Int., 35, 1234–1242, doi:10.1016/j.envint.2009.07.002, 2009.

Makowski Giannoni, S., Rollenbeck, R., Fabian, P., and Bendix, J.: Complex topography influences atmospheric nitrate deposition in a neotropical mountain rainforest, Atmos. Environ., 79, 385–394, doi:10.1016/j.atmosenv.2013.06.023, 2013.
Menz, F. C. and Seip, H. M.: Acid rain in Europe and the United States: an update, Environ. Sci. Policy, 7, 253–265, doi:10.1016/j.envsci.2004.05.005, 2004.
Morales, J., Bifano, C., and Escalona, A.: Atmospheric deposition of SO_4–S and (NH_4+NO_3)–N at two rural sites in the Western Maracaibo Lake Basin, Venezuela, Atmos. Environ., 32, 3051–3058, available at: http://www.sciencedirect.com/science/article/pii/S135223109700160X (last access: 21 August 2012), 1998.
Mu, M., Randerson, J. T., Van der Werf, G. R., Giglio, L., Kasibhatla, P., Morton, D., Collatz, G. J., DeFries, R. S., Hyer, E. J., PRINS, E. M., Griffith, D. W. T., Wunch, D., Toon, G. C., Sherlock, V., and Wennberg, P. O.: Daily and 3-hourly variability in global fire emissions and consequences for atmospheric model predictions of carbon monoxide, J. Geophys. Res., 116, D24303, doi:10.1029/2011JD016245, 2011.
Pauliquevis, T., Lara, L. L., Antunes, M. L., and Artaxo, P.: Aerosol and precipitation chemistry measurements in a remote site in Central Amazonia: the role of biogenic contribution, Atmos. Chem. Phys., 12, 4987–5015, doi:10.5194/acp-12-4987-2012, 2012.
Pfeffer, M. A., Langmann, B., and Graf, H.-F.: Atmospheric transport and deposition of Indonesian volcanic emissions, Atmos. Chem. Phys., 6, 2525–2537, doi:10.5194/acp-6-2525-2006, 2006.
Phoenix, G. K., Hicks, K. W., Cinderby, S., Kuylenstierna, J. C. I., Stock, W. D., Dentener, F. J., Giller, K. E., Austin, A. T., Lefroy, R. D. B., Gimeno, B. S., Ashmore, M. R., and Ineson, P.: Atmospheric nitrogen deposition in world biodiversity hotspots: the need for a greater global perspective in assessing N deposition impacts, Glob. Change Biol., 12, 470–476, doi:10.1111/j.1365-2486.2006.01104.x, 2006.
Prins, E. M. and Menzel, W. P.: Geostationary satellite detection of biomass burning in South America, Int. J. Remote Sens., 13, 2783–2799, doi:10.1080/01431169208904081, 1992.
Rissler, J., Vestin, A., Swietlicki, E., Fisch, G., Zhou, J., Artaxo, P., and Andreae, M. O.: Size distribution and hygroscopic properties of aerosol particles from dry-season biomass burning in Amazonia, Atmos. Chem. Phys., 6, 471–491, doi:10.5194/acp-6-471-2006, 2006.
Rodrigues-Ramos, A., Prado do Nascimento, E., and Oliveira, M.: Temporada de incêndios florestais no Brasil em 2010: análise de série histórica de 2005 a 2010 e as influências das chuvas e do desmatamento na quantidade dos focos de calor, in Simpósio Brasileiro de

Sensoriamento Remoto, 7902–7909, Curitiba, available at: http://www.dsr.inpe.br/sbsr2011/files/p1414.pdf (last access: 23 May 2014), 2011.
Rollenbeck, R.: Global sources-local impacts: natural and anthropogenic sources of matter deposition in the Andes of Ecuador, Geo-öko, 31, 5–27, 2010.
Rollenbeck, R., Fabian, P., and Bendix, J.: Precipitation dynamics and chemical properties in tropical mountain forests of Ecuador, Adv. Geosci., 6, 73–76, doi:10.5194/adgeo-6-73-2006, 2006.
Rollenbeck, R., Bendix, J., Fabian, P., Boy, J., Wilcke, W., Dalitz, H., Oesker, M., and Emck, P.: Comparison of different techniques for the measurement of precipitation in tropical montane rain forest regions, J. Atmos. Ocean. Tech., 24, 156–168, doi:10.1175/JTECH1970.1, 2007.
Rollenbeck, R., Bendix, J., and Fabian, P.: Spatial and temporal dynamics of atmospheric water inputs in tropical mountain forests of South Ecuador, Hydrol. Process., 25, 344–352, doi:10.1002/hyp.7799, 2011.
Rudel, T. K., Coomes, O. T., Moran, E., Achard, F., Angelsen, A., Xu, J., and Lambin, E.: Forest transitions: towards a global understanding of land use change, Global Environ. Chang., 15, 23–31, doi:10.1016/j.gloenvcha.2004.11.001, 2005.
Schemenauer, R. S. and Cereceda, P.: A proposed standard fog collector for use in high-elevation regions, J. Appl. Meteorol., 33, 1313–1322, doi:10.1175/1520-0450(1994)033<1313:APSFCF>2.0.CO;2, 1994.
Sigha-Nkamdjou, L., Galy-Lacaux, C., Pont, V., Richard, S., Sighomnou, D., and Lacaux, J.: Rainwater chemistry and wet deposition over the equatorial forested ecosystem of Zoétélé (Cameroon), J. Atmos. Chem., 46, 173–198, doi:10.1023/A:1026057413640, 2003.
Smith, S. J., van Aardenne, J., Klimont, Z., Andres, R. J., Volke, A., and Delgado Arias, S.: Anthropogenic sulfur dioxide emissions: 1850–2005, Atmos. Chem. Phys., 11, 1101–1116, doi:10.5194/acp-11-1101-2011, 2011.
Stevenson, D. S., Johnson, C. E., Collins, W. J., and Derwent, R. G.: The tropospheric sulphur cycle and the role of volcanic SO_2, Geological Society, London, Special Publications, 213, 295–305, doi:10.1144/GSL.SP.2003.213.01.18, 2003.
Stuefer, M., Freitas, S. R., Grell, G., Webley, P., Peckham, S., McKeen, S. A., and Egan, S. D.: Inclusion of ash and SO_2 emissions from volcanic eruptions in WRF-Chem: development and some applications, Geosci. Model Dev., 6, 457–468, doi:10.5194/gmd-6-457-2013, 2013.

ACPD
14, 13869–13908, 2014

Torres, O., Chen, Z., Jethva, H., Ahn, C., Freitas, S. R., and Bhartia, P. K.: OMI and MODIS observations of the anomalous 2008–2009 Southern Hemisphere biomass burning seasons, Atmos. Chem. Phys., 10, 3505–3513, doi:10.5194/acp-10-3505-2010, 2010.

Van der Werf, G. R., Randerson, J. T., Giglio, L., Collatz, G. J., Mu, M., Kasibhatla, P. S., Morton, D. C., DeFries, R. S., Jin, Y., and van Leeuwen, T. T.: Global fire emissions and the contribution of deforestation, savanna, forest, agricultural, and peat fires (1997–2009), Atmos. Chem. Phys., 10, 11707–11735, doi:10.5194/acp-10-11707-2010, 2010.

Wullaert, H., Homeier, J., Valarezo, C., and Wilcke, W.: Response of the N and P cycles of an old-growth montane forest in Ecuador to experimental low-level N and P amendments, Forest Ecol. Manag., 260, 1434–1445, doi:10.1016/j.foreco.2010.07.021, 2010.

ACPD
14, 13869–13908, 2014

S. Makowski Giannoni et al.

Table 1. pH and conductivity summary statistics in Occult Precipitation (OP) and rain samples from *El Tiro* and *Cerro del Consuelo* Meteorological Stations (MSs). MAD stands for Median Absolute Deviation.

	El Tiro		*Cerro del Consuelo*	
	OP	Rain	OP	Rain
Median pH	4.8	5.41	5	5.3
Min–max pH	2.4–5.8	3.7–6.7	1.8–6.2	3–6.1
	MAD = 0.37	MAD = 0.51	MAD = 0.29	MAD = 0.36
Median conductivity ($S\,m^{-1}$)	10.9	3.7	2.6	8.1
	MAD = 6.4	MAD = 1.6	MAD = 1	MAD = 6.8
Min–max conductivity ($S\,m^{-1}$)	2.3–110.3	1.4–45.4	1.4–12.4	1.7–72

ACPD
14, 13869–13908, 2014

Table 2. Cross-correlation of calculated SO_2 concentration time-series over *El Tiro* and *Cerro del Consuelo* SO_2 transport pixels using the different emission data sets.

	B. burning (GFED SO_2)	Regional volcanic and strong anthropogenic (OMI SO_2)	Volcanic (Aerocom SO_2)	Anthropogenic (EDGAR SO_2)
(a) Pixel *El Tiro*				
B. burning (GFED SO_2)	1			
Regional volcanic and strong anthropogenic (OMI SO_2)	0.01	1		
Volcanic (Aerocom SO_2)	0.14	0.42[a]	1	
Anthropogenic (EDGAR SO_2)	−0.29[c]	0.52[a]	0.66[a]	1
(b) Pixel *Cerro del C.*				
B. burning (GFED SO_2)	1			
Regional volcanic and strong anthropogenic (OMI SO_2)	−0.13	1		
Volcanic (Aerocom SO_2)	0.13	0.60[a]	1	
Anthropogenic (EDGAR SO_2)	−0.35[b]	0.69[a]	0.76[a]	1

[a] $p < 0.001$
[b] $p < 0.01$
[c] $p < 0.05$

ACPD
14, 13869–13908, 2014

On the origin of atmospheric sulfate

S. Makowski Giannoni et al.

Table 3. Cross-correlation matrix for SO_2 transport concentrations above *El Tiro* and *Cerro del Consuelo* pixels and sulfate concentrations from Meteorological Stations (MSs) of these two sites, located on a mountain pass upriver and on the highest catchment peak, respectively. Variables in bold represent measured sulfate (SO_4^-) concentrations and non-bold variables SO_2 transport. OP stands for occult precipitation.

	B. burning	Regional volcanic and strong anthropogenic (OMI SO_2)	Volcanic (Aerocom SO_2)	Anthropogenic (EDGAR SO_2)
OP SO_4^- (*El Tiro*)	0.43[a]	0.40[b]	0.18	0.19
Rain SO_4^- (*El Tiro*)	0.08	0.33[c]	0.39[b]	0.46[a]
OP SO_4^- (*C. del Consuelo*)	0.27	0.43[b]	0.52[a]	0.37[b]
Rain SO_4^- (*C. del Consuelo*)	0.21	0.09	0.12	0.14

[a] $p < 0.001$
[b] $p < 0.01$
[c] $p < 0.05$

Discussion Paper | Discussion Paper | Discussion Paper | Discussion Paper |
ACPD
14, 13869–13908, 2014

Table 4. Eigenvectors and communalities from factor analysis with varimax rotation, where (a) shows the results of the data aggregated according to *Cerro del Consuelo* Meteorological Station (MS) sample collection dates and (b) those for *El Tiro* MS.

a) Eigenvectors	Factor 1	Factor 2	Factor 3	Factor 4	Factor 5	Factor 6
GFED SO_2	0.14	0.61	0.69	0.12	0.28	0.12
OMI SO_2	−0.48	−0.08	0.27	0.65	−0.40	−0.31
Aerocom SO_2	−0.51	−0.07	0.16	−0.44	0.46	−0.55
EDGAR SO_2	−0.53	−0.21	−0.02	0.17	0.39	0.70
Cerro del C. SO_4^-	−0.42	0.41	−0.005	−0.5	−0.58	0.25
Cerro del C. SO_4^-	−0.16	0.63	−0.64	0.30	0.23	−0.16
Communalities						
GFED SO_2	6 %	55 %	35 %	1 %	3 %	0 %
OMI SO_2	66 %	1 %	5 %	19 %	6 %	1 %
Aerocom SO_2	76 %	1 %	2 %	9 %	8 %	5 %
EDGAR SO_2	79 %	6 %	0 %	1 %	6 %	8 %
Cerro del C. SO_4^-	50 %	25 %	0 %	11 %	13 %	1 %
Cerro del C. SO_4^-	7 %	56 %	30 %	4 %	2 %	0 %
b) Eigenvectors						
GFED SO_2	0.04	0.69	0.24	0.51	0.45	0.01
OMI SO_2	−0.47	0.1	−0.68	0	0.24	0.50
Aerocom SO_2	−0.47	−0.25	0.25	0.64	−0.46	0.17
EDGAR SO_2	−0.5	−0.33	0.02	0.03	0.52	0.60
Cerro del C. SO_4^-	−0.34	0.56	−0.22	−0.18	−0.5	−0.48
Cerro del C. SO_4^-	−0.44	0.16	0.61	0.08	−0.53	0.34
Communalities						
GFED SO_2	0 %	75 %	4 %	14 %	7 %	0 %
OMI SO_2	56 %	1 %	34 %	0 %	2 %	7 %
Aerocom SO_2	56 %	10 %	5 %	22 %	7 %	1 %
EDGAR SO_2	64 %	17 %	0 %	0 %	9 %	10 %
Cerro del C. SO_4^-	30 %	50 %	4 %	2 %	8 %	6 %
Cerro del C. SO_4^-	50 %	4 %	28 %	15 %	0 %	3 %

ACPD
14, 13869–13908, 2014

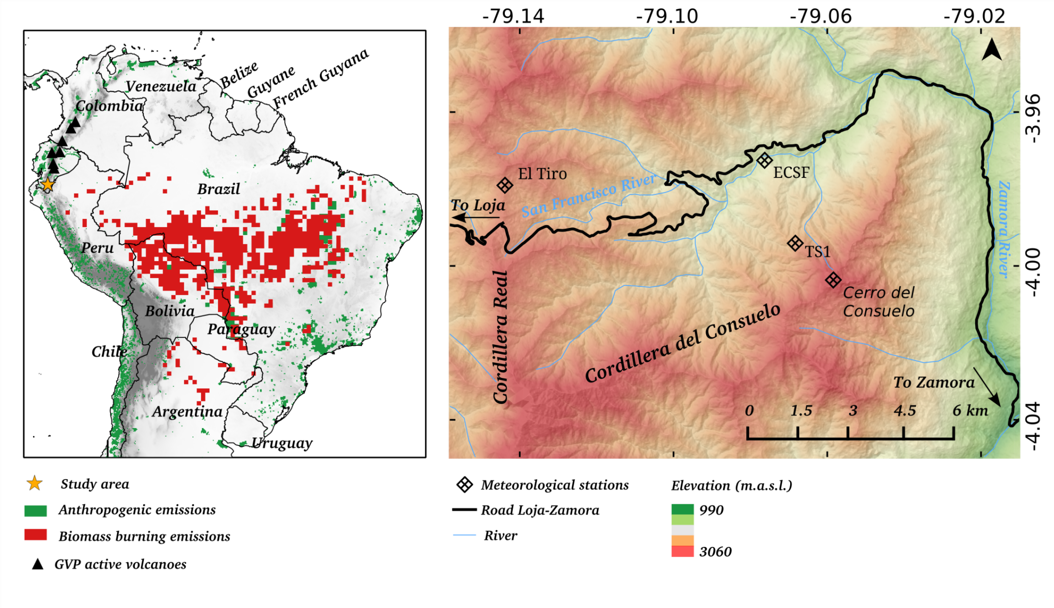

Figure 1. Study area. The left map shows possible anthropogenic and biomass-burning SO_2 sources in tropical South America and the location of active volcanoes in Ecuador and Colombia. The right map depicts the study area in the River San Francisco catchment and the location of the meteorological stations (MSs) involved in the study.

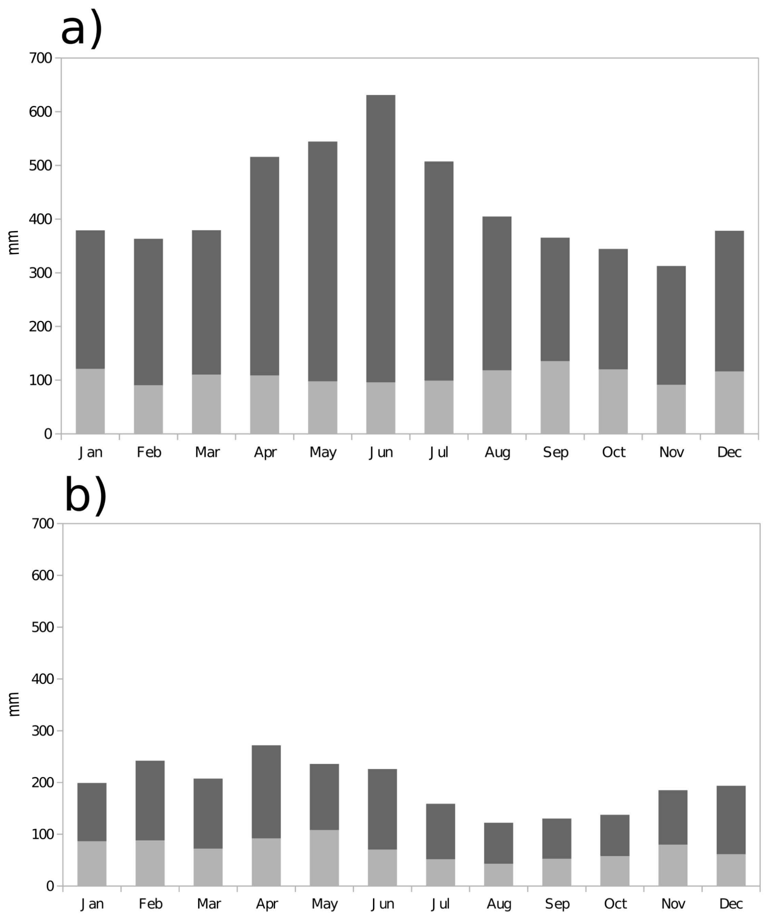

Figure 2. Rain (dark gray) and Occult Precipitation (OP) (light gray) monthly means for **(a)** *Cerro del Consuelo* and **(b)** *El Tiro* Meteorological Stations (MSs).

ACPD
14, 13869–13908, 2014

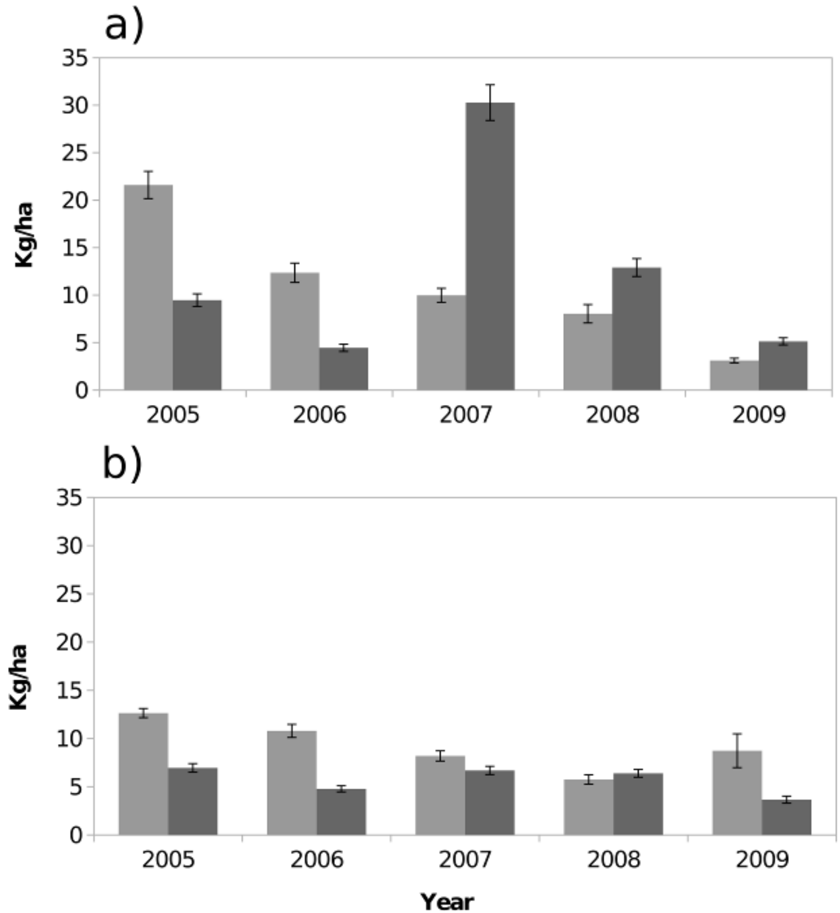

Figure 3. Total yearly sulfate (SO_4^-) deposition at **(a)** *Cerro del Consuelo* and **(b)** *El Tiro* MSs. Dark gray bars represent deposition by rain and light gray bars deposition by occult precipitation (OP).

ACPD
14, 13869–13908, 2014

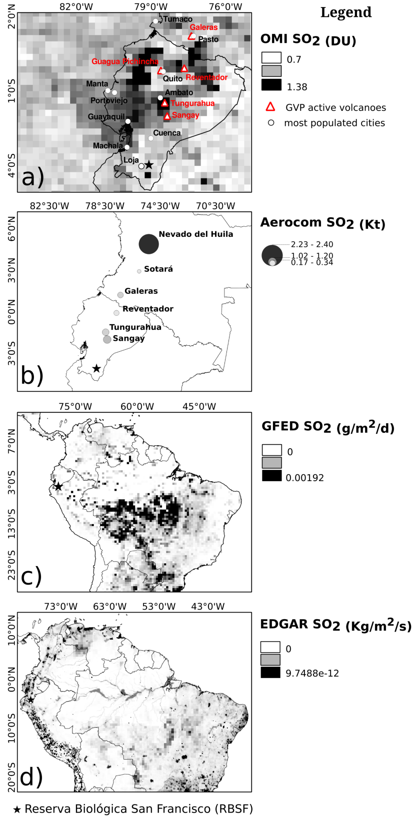

Figure 4. Average 2005–2009 source-dependent emission maps for **(a)** volcanic and strong anthropogenic regional emissions, **(b)** volcanic eruptive and passive degassing, **(c)** biomass-burning, and **(d)** anthropogenic emissions.

ACPD
14, 13869–13908, 2014

Title Page
Abstract
Introduction
Conclusions
References
Tables
Figures
◀▌ ▶▌
◀ ▶
Back
Close
Full Screen / Esc
Printer-friendly Version
Interactive Discussion

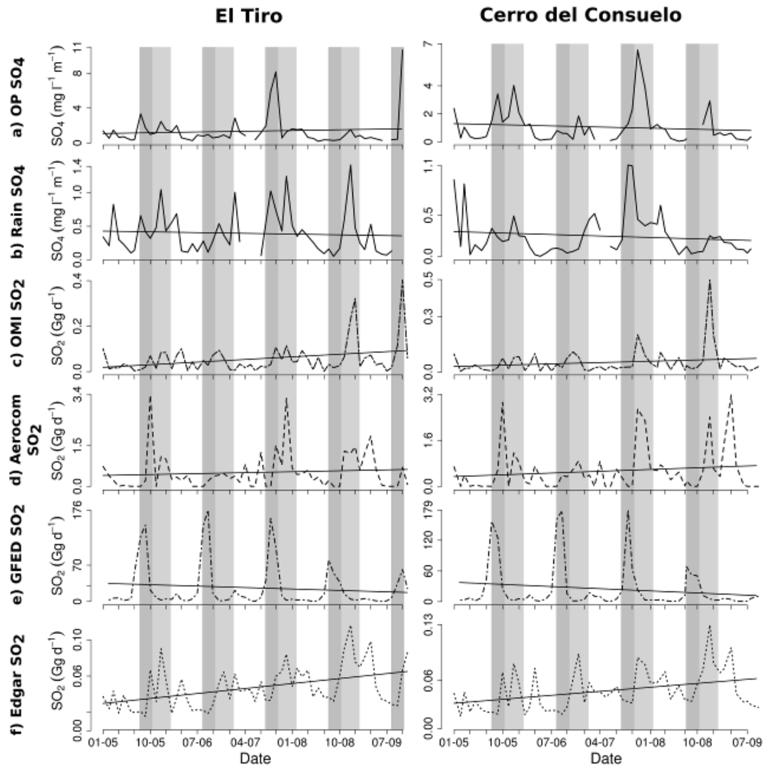

Figure 5. Time series comparing SO_2 transport from **(c)** volcanic and strong anthropogenic regional emissions (OMI), **(d)** volcanic emissions (Aerocom), **(e)** biomass-burning (GFED), and **(f)** anthropogenic emissions (EDGAR), to measured sulfate concentrations in **(a)** occult precipitation (OP) and **(b)** rain water from *Cerro del Consuelo* (right panel) and *El Tiro* (left panel) Meteorological Stations (Mss). The black straight line represents the tendency. Dark gray bars depict the Amazonian biomass-burning season (easterly wind direction) and light gray bars the shift of the incoming air masses to a northerly-northwesterly-westerly direction. Note the different scaling of the *y* axes.

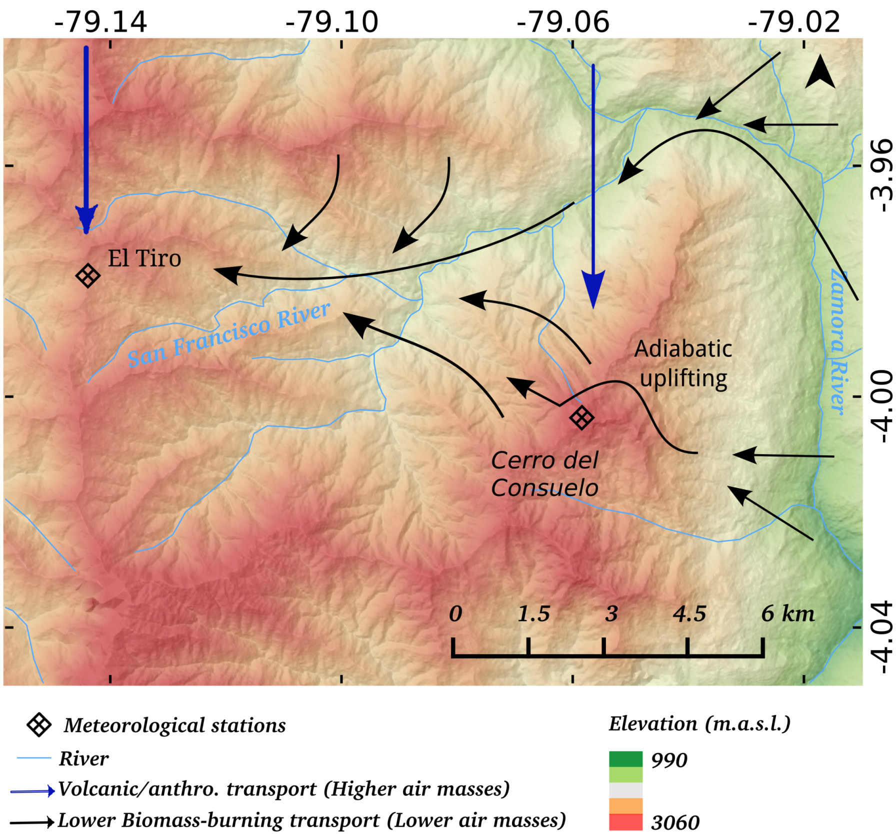

Figure 6. Conceptual sketch of the deposition regimes observed in the study area. The blue arrows represent volcanic and anthropogenic transport from the north and north-west creating rain deposition at *El Tiro* Meteorological Station (MS) and Occult Precipitation (OP) deposition at *Cerro del Consuelo* MS. The black arrows represent biomass-burning transport from the east creating OP deposition at *El Tiro* MS and mainly rain deposition at *Cerro del Consuelo* MS.

ACPD
14, 13869–13908, 2014

On the origin of atmospheric sulfate

S. Makowski Giannoni et al.